ACS APPLIED MATERIALS & INTERFACES

Research Article

www.acsami.org

Enhanced Performance of Polymeric Bulk Heterojunction Solar Cells via Molecular Doping with TFSA

Yubin Xiao,[†] Han Wang,[†] Shuang Zhou,[†] Keyou Yan,[†] Zhiqiang Guan,[‡] Sai-Wing Tsang,*[,‡] and Jianbin Xu*[,†]

[†]Department of Electronic Engineering and Materials Science and Technology Research Centre, The Chinese University of Hong Kong, Shatin, Hong Kong SAR, P. R. China

[‡]Department of Physics and Materials Science, The City University of Hong Kong, Kowloon Tong, Hong Kong SAR, P. R. China

Supporting Information

ABSTRACT: Organic solar cells based on bis(trifluoromethanesulfonyl)-amide (TFSA, $[CF_3SO_2]_2NH$) bulk doped poly[*N*-9′′-hepta-decanyl-2,7-carbazole-*alt*-5,5-(4′,7′-di-2-thienyl-2′,1′,3′-benzothiadiazole) (PCDTBT):C_{71}-butyric acid methyl ester ($PC_{71}BM$) were fabricated to study the effect of molecular doping. By adding TFSA (0.2−0.8 wt %, TFSA to PCDTBT) in the conventional PCDTBT:$PC_{71}BM$ blends, we found that the hole mobility was increased with the reduced series resistance in photovoltaic devices. The p-doping effect of TFSA was confirmed by photoemission spectroscopy that the Fermi level of doped PCDTBT shifts downward to the HOMO level and it results in a larger internal electrical field at the donor/acceptor interface for more efficient charge transfer. Moreover, the doping effect was also confirmed by charge modulated electroabsorption spectroscopy (CMEAS), showing that there are additional polaron signals in the sub-bandgap region in the doped thin films. With decreased series resistance, the open-circuit voltage (V_{oc}) was increased from 0.85 to 0.91 V and the fill factor (FF) was improved from 60.7% to 67.3%, resulting in a largely enhanced power conversion efficiency (PCE) from 5.39% to 6.46%. Our finding suggests the molecular doping by TFSA can be a facile approach to improve the electrical properties of organic materials for future development of organic photovoltaic devices (OPVs).

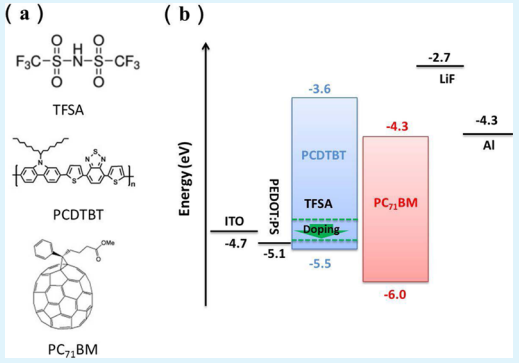

KEYWORDS: *polymer solar cells, TFSA doping, charge transfer, carrier mobility, Fermi level*

1. INTRODUCTION

The organic photovoltaic property has been an emerging technology during the past two decades due to its potential for low cost fabrication and high efficiency.[1] Particularly, solution-processable polymeric bulk heterojunction (BHJ) architecture has gained lots of attention due to the ease of fabrication processes. In the BHJ structure, an electron donating polymer and an electron acceptor (usually fullerene derivatives) are mixed together to form a nanoscale binary phase separation and a bicontinuous interpenetration network, which has significant contribution on facilitating efficient exciton dissociation.[2] Recently, the power conversion efficiency (PCE) of single BHJ solar cells has been reported to be over 10% in solution-processable solar cells which is approaching the threshold of 15% for commercialization.[3] Therefore, great effort is devoted to further improving the performance of polymer solar cells. The major drawbacks of BHJ-OPVs are often attributable to narrow light absorption band of the polymers, limited exciton migration, and low charge-carrier mobility. Hence, a relatively low open circuit voltage (V_{oc}) and a low fill factor (FF) are often observed in such organic solar cells. As V_{oc} is dependent on the energy gap between the lowest unoccupied molecular orbital (LUMO) of the acceptor and the highest occupied molecular orbital (HOMO) of the donor polymer, one strategy to increase the V_{oc} is to develop new polymers with relatively low-lying HOMO level, such as PCDTBT,[4−8] benzodithiophene polymers (PTBs),[9,10]etc. Another approach is to optimize the energetic alignment at the electrode/active layer interface to create an Ohmic contact, to reduce the charge recombination and to promote carrier collection.[11] Moreover, ternary solar cells have been developed to further enhance PCE by expanding the light absorption range and smoothing the energy level at the BHJ interface.[12−14]

It has been demonstrated that the electrical properties of the semiconducting polymers can be modified via molecular doping with charge transfer between the organic host and dopant molecules.[15−17] Also, molecular doping has been applied to enhance the photoconductivity and charge injection/collection efficiencies in BHJ-OPVs.[18−21] However, the choices of the dopant molecules used in polymeric materials are limited, as

Received: March 10, 2015
Accepted: June 3, 2015
Published: June 3, 2015

DOI: 10.1021/acsami.5b02104
ACS Appl. Mater. Interfaces 2015, 7, 13415−13421

these require good compatibility in solubility and efficient charge transfer. When doped with a prototypical p-type molecular dopant tetrafluoro-tetracyanoquinodimethane (F4-TCNQ), a doped polymer showed a downward shifted Fermi level and an increased carried density; as a result, the background hole carrier concentration was increased, contributing to an increased photoconductivity and a resultant improved PCE.[19,22] Another p-type dopant, molybdenum tris[1-(methoxycarbonyl)-2-(trifluoromethyl)-ethane-1,2-dithiolene] ($Mo(tfd\text{-}CO_2Me)_3$), has also been proven to be able to create an efficient hole-collecting contact in solution-processed inverted polymer solar cells.[11] Recently, a new dopant bis(trifluoromethanesulfonyl)amide (TFSA) has also been reported as a p-type dopant for carbonaceous materials (carbon nanotube, graphene) due to its strong electron affinity. A graphene-based Schottky junction solar cells doped with TFSA exhibited a PCE of 8.6%.[23] In addition, in polymer light emitting diodes, the work function of a graphene electrode was successfully increased by TFSA for efficient hole injection.[24]

In this contribution, we investigated the application of TFSA as molecular dopant in solution-processed BHJ-OPVs. By controlling the doping concentration (0.2−0.8 wt %, TFSA to PCDTBT), we found that the V_{oc} of the PCDTBT:$PC_{71}BM$ solar cells was increased from 0.85 to 0.91 V, FF was increased from 60.7% to 67.3%, and an enhanced PCE from 5.39% to 6.46% was further achieved. Employing different spectroscopy techniques, we found that there is efficient charge transfer between PCDTBT and TFSA, which enables the modification of electrical properties and energy level alignment in the photovoltaic devices. The results demonstrate the capability of TFSA as an efficient molecular dopant used in polymeric BHJ-OPVs.

2. EXPERIMENTAL SECTION

PCDTBT, $PC_{71}BM$, and TFSA were purchased from 1-Material Chemscitech, Inc., Lumitec, and Sigma-Aldrich, respectively, and used as received. In order to demonstrate the effect of TFSA, the device with configuration of ITO (180 nm)/PEDOT:PSS(40 nm)/PCDTBT:$PC_{71}BM$ (~80 nm)/LiF (1 nm)/Al (100 nm) was fabricated. To begin, a prepatterned ITO (conductivity: 10−15 Ω/square) glass was cleaned by detergent, deionized water, acetone, and isopropanol in sequence, followed by oxygen plasma treatment for 90 s. A thin hole injection layer of PEDOT:PSS was spun-cast onto precleaned ITO glass with a thickness of ca. 40 nm, and then annealed at 145 °C for 10 min in air. PCDTBT and $PC_{71}BM$ with a mass ratio of 1:3 were dissolved in a mixed solution composed of 1,2 *o*-dichlorobenzene (o-DCB) and chloroform (CF) (1:1 vol) with a total concentration of 29 mg/mL. TFSA was dissolved in 1 mL of 1,2 *o*-dichlorobenzene (o-DCB) and chloroform (CF) (1:1) mixed solvent, and then it was added to PCDTBT:$PC_{71}BM$ blends with the desired amount. The weight ratio of TFSA to PCDTBT is 0.2%, 0.4%, 0.6%, and 0.8%. The mixed solution was then spun-cast atop the precoated PEDOT:PSS layer to form the active layer, giving rise to a thickness of ~80 nm. Following that, 20 min of soft annealing and a further annealing at 120 °C for 10 min were conducted. Finally, a thin LiF interfacial layer (~1 nm) and a 100 nm thick Al electrode were deposited sequentially by thermal evaporation. The evaporator was BOC Edwards Auto 306, and the active layer area of the device was defined by a shadow mask of 2 mm × 6 mm.

Electrical measurements were performed by a semiconductor characterization system (Keithley 236) at room temperature in air under the spectral output from solar simulator (Newport) using an AM 1.5G filter with a light power of 100 mW/cm^2. The light intensity was precisely calibrated by a calibrated silicon solar cell. The morphologies of the PCDTBT:$PC_{71}BM$ blend thin films were characterized by atomic force microscopy (AFM) in tapping mode (Dimension icon scanasyst). The thicknesses of the active layer and evaporated layers were recorded with a thickness monitor (Sigma SQM-160), and also verified by AFM. The impedance were measured in a frequency range from 0.1 Hz to 1 MHz (CHI 760). The admittance, capacitance−voltage ($C-V$), and capacitance−frequency ($C-F$) characteristics were measured by HP Hewlett Packard 4248A. Especially for the $C-F$ measurement, a very thick PCDTBT layer (500 nm) was prepared in order to sweep out the relaxation peak in the $-\Delta B$ versus f plots. UPS measurement was also conducted, and the Fermi energy level of PCDTBT is determined by $E = h\nu - E_{onset}$, where $h\nu$ is the energy of the ultraviolet irradiation with the value of 21.22 eV. A −5 V bias voltage was applied on ITO electrode in order to separate the low cutoff energy levels of the secondary photoelectrons from the spectral edge of UPS. The testing devices for CMEAS have the structure of ITO/PCDTBT/LiF/Al, and the measurements were carried out at room temperature. A monochromatic parallel beam probed the devices through the ITO side with an incident angle of 45° and was reflected by the back Al electrode. Calibrated silicon and germanium photodetectors were used to detect the reflected signals.

3. RESULTS AND DISCUSSION

Figure 1a shows the materials in the study, and the doping process is illustrated in Figure 1b; after the addition of TFSA to

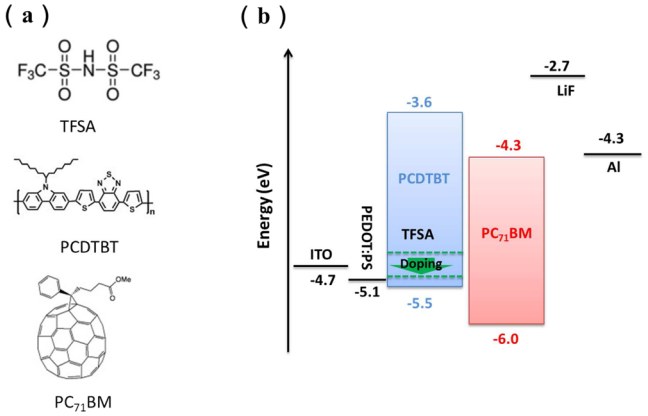

Figure 1. (a) Chemical structure of TFSA, PCDTBT, and $PC_{71}BM$ used in the study. (b) Energy diagram of the BHJ solar cell. With the p-type doping, the green arrow indicates the Fermi level of PCDTBT shifted toward its HOMO level.

PCDTBT:$PC_{71}BM$ blends, the electron will transfer from PCDTBT to TFSA due to the strong electron affinity of TFSA. Becasue of the electron lost in PCDTBT, the work function of PCDTBT will move downward and closer to its HOMO energy level as indicated by the green arrow. As a result, the hole concentration in the donor polymer will increase. Such a phenomenon is confirmed by $C-V$ characteristics and photoemission spectroscopy measurements that will be discussed later.

The influence of TFSA dopants on the morphological properties of the photoactive layer was examined by atomic force microscopy (AFM). Figure 2 shows the 2 μm × 2 μm AFM topographic images of bare PCDTBT:$PC_{71}BM$ films as well as the TFSA-doped films (0.2−0.8%). For pristine PCDTBT:$PC_{71}BM$, it shows a very smooth and featureless structure with a low root-mean-square (RMS) value of 0.49 nm, while for doped films, the RMS displays slightly inceased value to 0.50, 0.51, 0.52, and 0.53 nm at each doping concentration, respectively. Also, the minor variation of the film morphology would have negligible impact to the polymer film properties.

DOI: 10.1021/acsami.5b02104
ACS Appl. Mater. Interfaces 2015, 7, 13415−13421

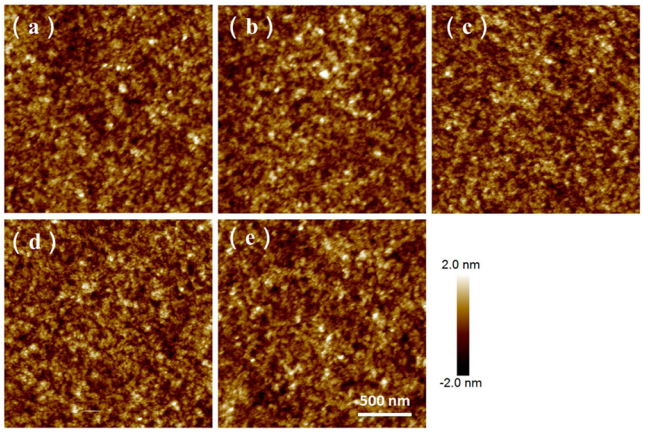

Figure 2. AFM morphology images of PCDTBT:$PC_{71}BM$: (a) pristine and with (b) 0.2%, (c) 0.4%, (d) 0.6%, (e) 0.8% TFSA dopant.

From the corresponding phase images (Supporting Information Figure S1), no obvious ternary TFSA domain was obseved, indicating small dopant concentration would not change the PCDTBT:$PC_{71}BM$ interpenetrating network. Although AFM is only a surface sensitive technique, it provides useful insight into the bulk information on the active layers. From the above morphological and phase images, we can expect that the variation of the photoactive layer properties could be neglected at low doping concentration due to the nearly unchanged film construction.

Next, we studied the influence of molecular doping by TFSA on the performance of the photovoltaic effect. Figure 3a shows typical current density versus voltage (J–V) characteristics of PCDTBT:$PC_{71}BM$ solar cells under AM 1.5 G illumination. For pristine PCDTBT:$PC_{71}BM$ solar cells, it displays a V_{oc} of 0.85 V, a short circuit current (J_{sc}) of 10.5 mA/cm^2, and a FF of 60.7%. All of the above give rise to a PCE of 5.39%. With addition of TFSA, a noticeable enhancement of V_{oc} and FF are observed, while J_{sc} is insensitive to the TFSA doping at various concentrations. The detailed device characteristics are listed in Table 1. In the device adding only 0.2% TFSA, the V_{oc} is increased to 0.89 V, and FF is increased to 63.0%. When adding 0.4% TFSA, the device reaches its optimized performance with a V_{oc} of 0.91 V, a FF of 67.3%, and a PCE to 6.46%. As discussed previously, the doped PCDTBT has a low work function due to electron tranfer to TFSA and results in an optimized energy level alignment; thus, the charge injection barrier could therefore be reduced at the ITO–active layer interface. To further confirm the enhancement at lower doping concentration, devices with and without the optimized condition of 0.4% TFSA dopant (both devices without PEDOT:PSS hole injection layer) were fabricated (see Figure S2 in Supporting Information). Similarly, the V_{oc} was increased from 0.40 to 0.58 V, and FF increased slightly from 42.9% to 44.0%. The results of this simple device structure without hole transporting layer (HTL) confirmed that the doped device provided a better charge transfer path across the electrode-active layer junction due to the reduced charge injection barrier. However, when increasing the dopant concentration to 0.6% and 0.8%, the device performance rolled-off; this is similar to the previous report that the low to medium doping concentration reduced the carrier mobility.[25,26]

Figure 3b shows the dark current versus bias voltage characteristics of the PV devices. At low doping concentrations, the dark current at reverse bias and leakage current at zero bias are obviously reduced, which significantly increases the diode rectifying ratios by 2 orders of magnitude. The decreased dark current indicates a larger shunt resistance (R_{sh}) that could prevent the current from leakage and hence increase the V_{oc} and FF. While the dark current in the forward bias region (1–2 V) was dominated by fast carriers of electrons, the currents are barely changed, indicating that doping in PCDTBT:$PC_{71}BM$ films with low dopant concentrations does not affect the electron transportation. Previous works have also shown that a low doping molecular concentration had less impact on the carrier transportation and the enhanced carrier concentration would not lead to a detrimental charge recombination.[22,27]

Molecular doping with extra carriers would lead to lower resistance in PV devices. Figure 4 shows the Nyquist curves of the impedance spectra for undoped and doped PCDTBT:$PC_{71}BM$ PV devices measured at the open circuit voltage condition. An apparent change is observed in the doped devices. The real impedance is decreased from 1011 Ω to 918, 352, and 701 Ω as doping concentrations are increased from 0.2 to 0.6 wt %, respectively. This can be attributed to the contribution of both carrier concentration and carrier mobility. In order to further investigate the impact of molecular doping on the electrical properties of PCDTBT:$PC_{71}BM$ solar cells, we used admittance spectroscopy to measure the carrier mobility and carrier transit time in those devices.[28,29] The carrier mobility can be exacted from the relation of $\mu_{dc} = d^2/(\tau_{dc}V_{dc})$,

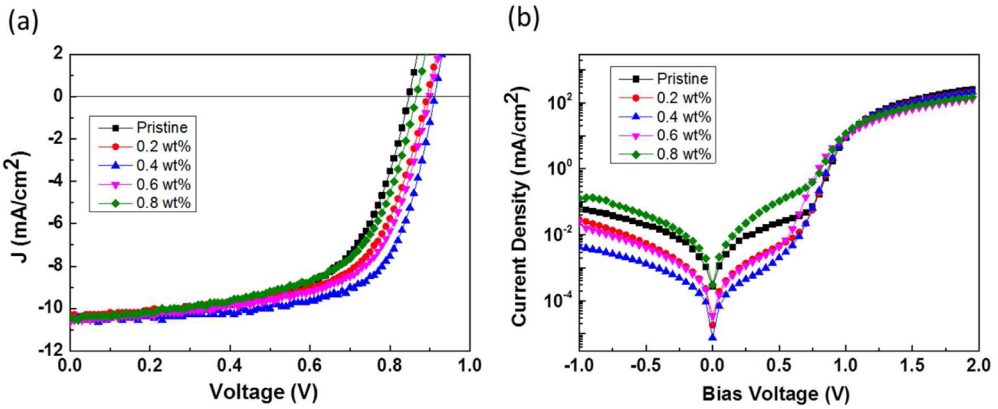

Figure 3. (a) Current density versus voltage characteristics of PCDTBT:$PC_{71}BM$ solar cells under 100 mW/cm^2 irradiation. (b) Dark current density versus voltage.

DOI: 10.1021/acsami.5b02104
ACS Appl. Mater. Interfaces 2015, 7, 13415–13421

Table 1. Photovoltaic Parameters, Hole Concentration of PCDTBT:$PC_{71}BM$ Solar Cells, and Mobility of PCDTBT Thin Film with Various TFSA Dopant Concentrations[a]

	V_{oc} (V)	J_{sc} (mA/cm^2)	FF (%)	PCE (%)	$N_A \times 10^{17}$ cm^{-3}	mobility $\times 10^{-4}$ (cm^2/(V s))
pristine	0.85 ± 0.02	10.5 ± 0.1	60.7 ± 0.1	5.39 ± 0.01	1.0	6.2
0.2 wt %	0.89 ± 0.02	10.3 ± 0.2	63.0 ± 0.4	5.76 ± 0.01	1.7	7.4
0.4 wt %	0.91 ± 0.01	10.5 ± 0.1	67.3 ± 0.2	6.46 ± 0.03	3.1	9.2
0.6 wt %	0.90 ± 0.02	10.6 ± 0.1	62.2 ± 0.3	5.96 ± 0.02	4.8	8.0
0.8 wt %	0.87 ± 0.03	10.5 ± 0.2	59.2 ± 0.5	5.37 ± 0.04	6.0	5.9

[a]Average was obtained from over 20 devices tested.

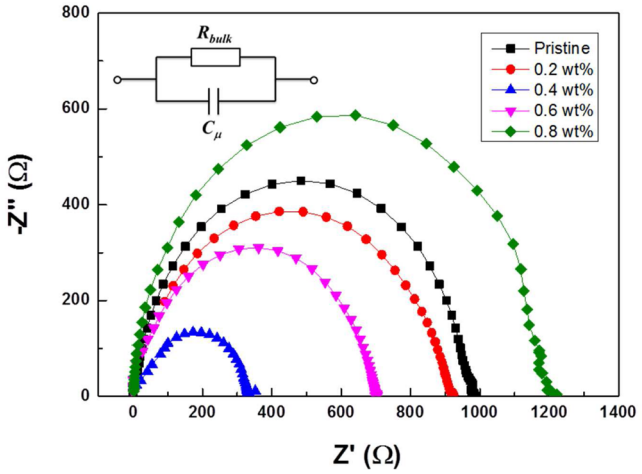

Figure 4. Nyquist plots of impedance spectra for PCDTBT:$PC_{71}BM$ solar cells without and with TFSA treatment at various concentrations and measured at the V_{oc} condition under dark. Inset shows the equivalent circuits of the devices, where R_{bulk} is the bulk resistance and C_μ the chemical capacitance.

where d is the thickness of the polymer and V_{dc} is the external applied bias voltage. Hence, from the relationship mentioned above, the carrier mobility and transit time can be extracted. The hole-only devices were fabricated with the structure ITO/PEDOT:PSS/PCDTBT/MoO_3/Al. MoO_3 is an electron blocking layer here. Figure 5a–c and Figure 5d–f) present the impedance analysis of control and 0.4% TFSA-doped devices with a bias voltage range from 3 to 12 V, respectively. Apparently, the doped devices display an enhanced conductance at each voltage bias. The results are summarized in Table 2. With the typical bias V_{dc} at 10 V as an example, the carrier mobility is increased from 6.7×10^{-4} to 8.9×10^{-4} cm^2/(V s), and the conductance from 37 to 150 μS. The higher carrier mobility in the slightly doped device suggests more efficient charge extraction.

To confirm the increased carrier mobility, J–V characteristics were examined in a bias voltage range 0–10 V (Supporting Information Figure S3) for undoped and doped PCDTBT:$PC_{71}BM$ hole-only devices. With positive bias applied on an ITO anode, holes are injected into PCDTBT, and the space charge limited current (SCLC) occurs.[30] Also, the mobility can be extracted from the Mott–Gurney equation

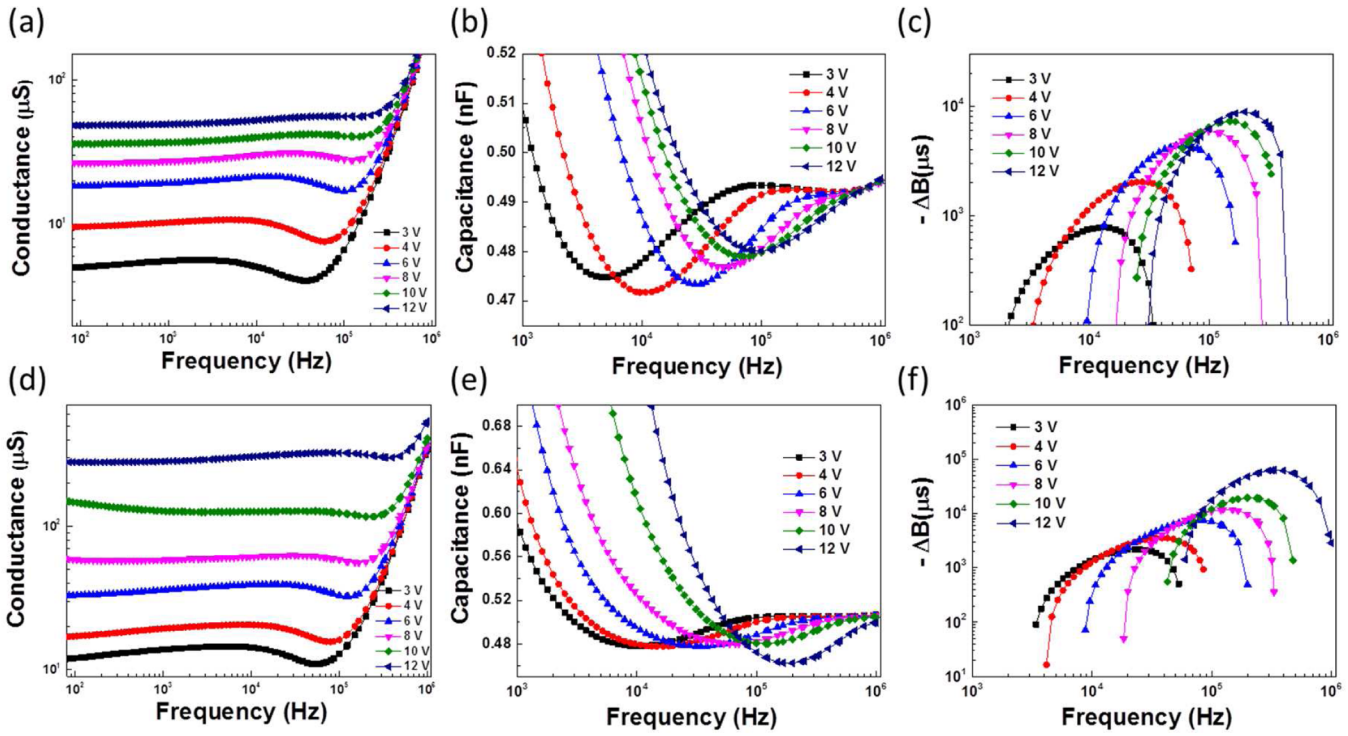

Figure 5. (a, d) Conductance, (b, e) capacitance, and (c, f) negative differential susceptances $-\Delta B$ of pristine and 0.4% TFSA-doped PCDTBT hole-only devices, respectively. $-\Delta B$ is derived from capacitance data in parts b and d, by the following equation: $-\Delta B = -\omega(C - C_{geo})$, where $f = \omega/2\pi$, C, and C_{geo} are the frequency dependent and geometric capacitances of the organic film, respectively.

DOI: 10.1021/acsami.5b02104
ACS Appl. Mater. Interfaces 2015, 7, 13415–13421

Table 2. Carrier Average Mobility and Average Transit Time from Admittance Spectroscopy Analysis

	mobility × 10^{-4} (cm^2/(V s))		transit time (μs)	
	pristine	0.4% doped	pristine	0.4% doped
3 V	2.0	3.4	42.1	24.6
4 V	3.1	4.3	20.2	14.6
6 V	5.0	6.0	8.4	7.0
8 V	5.6	7.0	5.6	4.5
10 V	6.7	8.9	3.8	2.8
12 V	7.4	12.4	2.8	1.7

$$\mu = \frac{8d^3}{9\varepsilon_0\varepsilon_r}\left(\frac{\sqrt{J}}{V_a}\right)^2$$

where μ is the carrier mobility, d is the active layer thickness, and ε_0 (8.85×10^{-12} F/m) and ε_r (equal to 3 for organic materials) are the permittivity of vacuum and relative permittivity, respectively. According to the above equation, the hole mobility of the control device is 6.2×10^{-4} cm^2/(V s), and after adding TFSA, the hole mobility is gradually increased. With 0.4% TFSA doped, the hole mobility achieves 9.2×10^{-4} cm^2/(V s) which is in good agreement with the admittance analysis results. However, when the doping concentration is increased to 0.8%, the hole mobility is decreased to 5.9×10^{-4} cm^2/(V s) compared to the undoped device. This decreasing tendency is rationalized by an analytic model of carrier mobility in doped organic semiconductors by D. Heher et al.[25] To explore the doping effect of TFSA on PCDTBT, the UPS measurements were carried out at various concentrations, and the results are shown in Figure 6. The cutoff energy level of

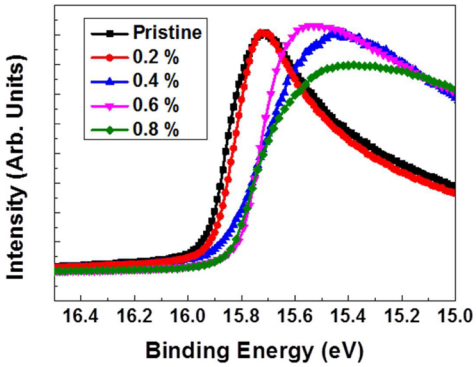

Figure 6. UPS spectra of pristine and TFSA-doped PCDTBT film as concentrations vary from 0.2% to 0.8%.

TFSA-doped PCDTBT shifts from 15.90 eV to lower binding energy level of 15.85 eV at 0.2% and saturates at 15.73 eV for the rest of the doping concentrations (0.4–0.8%), suggesting an increase of work function from 5.32 to 5.37 and 5.49 eV, respectively. Because the HOMO level of PCDTBT is around 5.5 eV, it clearly shows that, after doping with TFSA, the Fermi level of PCDTBT shifts downward effectively and leads to a larger effective bandgap at the donor/acceptor interface, and the enlarged effective bandgap should be one of the reasons for the increased open circuit voltage.

In order to extract the carrier concentration, we measured the capacitance–voltage characteristic of the devices and compared the result with the Mott–Schottky relation $C^{-2} = 2(V_{bi} - V)/A^2 q\varepsilon_0\varepsilon_r N_A$, where A is the device area (0.12 mm^2), ε_r and ε_0 are the relative dielectric constant and permittivity of vacuum, respectively, q the elementary charge, N_A the concentration of impurities. Figure 7 shows the $C-V$ characteristics and Mott–Schottky curves of PCDTBT:$PC_{71}BM$ solar cells with and without TFSA doping at various concentrations. Having similar device thickness, higher capacitance is obtained after doping with TFSA as shown in Figure 7a. It suggests a higher carrier concentration corresponding to charge transfer between TFSA and PCDTBT. It should also be noted that the increased built-in potential (V_{bi}) after doping with TFSA is in good agreement with the improved V_{oc} in PV devices as shown above. We extract the carrier concentration from the linear region from the plots with different doping ratios. For pristine PCDTBT:$PC_{71}BM$ device, we obtain N_A at around 1.0×10^{17} cm^{-3}, and in 0.2% TFSA-doped device, N_A is increased to 1.7×10^{17} cm^{-3}. Thereafter, N_A stays increased as more TFSA added. The carrier concentrations for each doping concentration are summarized in Table 1, where N_A is proportional to the doping concentration.

To further figure out the doping effect of TFSA in PCDTBT, charge modulated electroabsorption spectroscopy (CMEAS) was employed to investigate the change of absorption due to additional polaron states in the doped devices.[31,32] In CMEAS measurement, by measuring the electroabsorption (EA) signal that is induced by charge modulation (CM) in the polymer, a clear sub-bandgap signal through direct excitation of excitons to the charge transfer states can be observed. Therefore, if there is charge transfer between TFSA and PCDTBT, the photogenerated carriers will couple with the modulating electric field and generate subtle changes in the optical absorption cross section in the sub-bandgap region, where an additional sub-bandgap signal in the infrared region should be observed in CMEAS measurement. Figure 8a shows the CMEAS spectra of pristine PCDTBT and TFSA-doped PCDTBT films. The excitonic feature of PCDTBT appearing above 1.8 eV is ascribed to the Stark effect due to the coupling between the excitonic level ($1B_u$) and the higher forbidden states under the applied electric field. In the doped PCDTBT device (Figure 8b), additional polaron signals in the sub-bandgap region from 1.0 to 1.8 eV are observed. This further confirms the efficient charge transfer between TFSA and PCDTBT.

Finally, we demonstrated the capability of molecular doping using TFSA in different polymer solar cells. Supporting Information Figure S4 shows the $J-V$ characteristics of solar cells based on poly(3-hexylthiophene-2,5-diyl) (P3HT):($PC_{61}BM$). With a doping concentration of 0.4%, an increased J_{sc} from 9.01 to 9.36 mA/cm^2 and a V_{oc} from 0.60 to 0.63 V are observed. As a result, the final PCEs are increased from 3.42% to 3.76% by doping with TFSA. The doping effect to polymer light absorption for both donors was investigated as well (Supporting Information Figure S5); it can be seen that, after mixing with TFSA, the light absorption shows a very similar tendency, indicating that the polymer structure is not affected by the dopant.

4. CONCLUSION

In summary, our TFSA-doped PCDTBT:$PC_{71}BM$ solar cell has significant improvement in both open circuit voltage and fill factor, leading to an improvement of PCEs from 5.39% to 6.46%. Impedance spectroscopy and admittance spectroscopy prove that the doped devices have higher carrier concentration and concentration dependent carrier mobility. Photoemission

DOI: 10.1021/acsami.5b02104
ACS Appl. Mater. Interfaces 2015, 7, 13415–13421

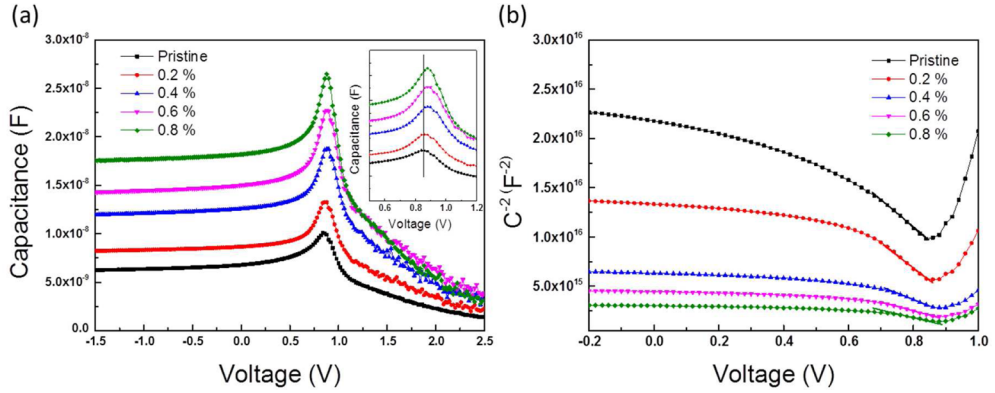

Figure 7. (a) $C-V$ characteristics and (b) Mott−Schottky curve of PCDTBT:$PC_{71}BM$ solar cells without and with TFSA treatment at various concentrations at frequency of 1 kHz. Inset in part a displays the V_{bi} position at each condition.

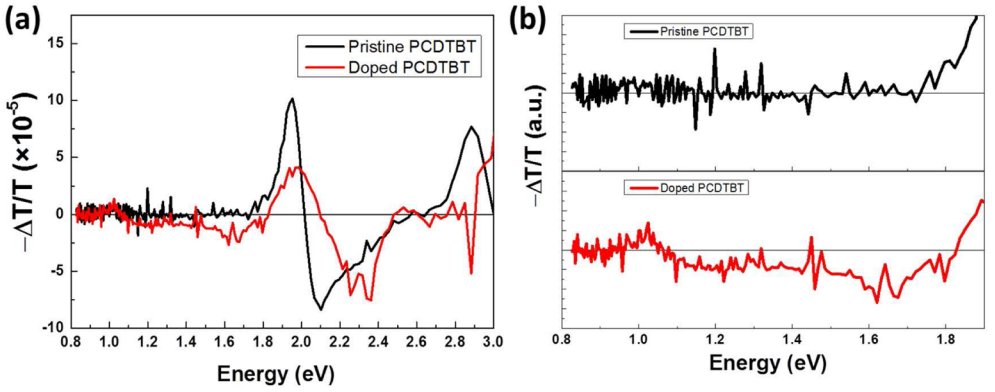

Figure 8. (a) Electroabsorption spectra of pristine and doped PCDTBT. (b) The sub-bandgap signal zoomed from part a at energy range from 0.8 to 1.9 eV.

spectroscopy results show the downward shifting of the Fermi level of PCDTBT after doping. Such charge transfer has also been confirmed by charge modulation spectroscopy that shows that additional polaron states are induced after doping. Our results demonstrate that TFSA can be used as an efficient doping molecule to further optimize the electrical properties of the polymeric based bulk heterojunction photovoltaic devices.

■ ASSOCIATED CONTENT

Supporting Information

AFM phase images of PCDTBT:$PC_{71}BM$ film, $J-V$ characteristics of PCDTBT:$PC_{71}BM$ without PEDOT:PSS, SCLC mobility, $J-V$ characteristics of P3HT:$PC_{61}BM$ solar cells, UV−vis spectroscopy, and EQE. The Supporting Information is available free of charge on the ACS Publications website at DOI: 10.1021/acsami.5b02104.

■ AUTHOR INFORMATION

Corresponding Authors

*For J.B Xu: E-mail: jbxu@ee.cuhk.edu.hk
*For S-W Tsang: E-mail: saitsang@cityu.edu.hk.

Notes

The authors declare no competing financial interest.

■ ACKNOWLEDGMENTS

This work is in part supported by Research Grants Council of Hong Kong, particularly, via Grants CUHK2/CRF/08, CUHK4182/09E, CUHK4179/10E, N-CUHK405/12, and AoE/P-03/08. J.X. would like to thank the National Science Foundation of China for the support, particularly via Grant 61229401. S.-W.T. would like to thank RGC-20101514 and CityU-9610309. We thank Dr. Fangyan Xie of the instrumental analysis and research center at Sun Yat-sen University for the UPS measurement.

■ REFERENCES

(1) Roncali, J.; Leriche, P.; Blanchard, P. Molecular Materials for Organic Photovoltaics: Small is Beautiful. *Adv. Mater.* **2014**, *26*, 3821−3838.
(2) Son, H. J.; Carsten, B.; Jung, I. H.; Yu, L. Overcoming Efficiency Challenges in Organic Solar Cells: Rational Development of Conjugated Polymers. *Energy Environ. Sci.* **2012**, *5*, 8158−8170.
(3) Liu, Y. H.; Li, Z. J.; Mu, C.; Ma, W.; Hu, H.; Jiang, K.; Lin, H. R.; Ade, H.; Yan, H. Aggregation and Morphology Control Enables Multiple Cases of High-Efficiency Polymer Solar Cells. *Nat. Commun.* **2014**, *5*, 5293−5300.
(4) Jia, X.; Shen, L.; Yao, M. N.; Liu, Y.; Yu, W. J.; Guo, W. B.; Ruan, S. P. Highly Efficient Low-Bandgap Polymer Solar Cells with Solution-Processed and Annealing-Free Phosphomolybdic Acid as Hole-Transport Layers. *ACS Appl. Mater. Interfaces* **2015**, *7*, 5367−5372.
(5) Yu, W. J.; Shen, L.; Shen, P.; Long, Y. B.; Sun, H. W.; Chen, W. Y.; Ruan, S. P. Semitransparent Polymer Solar Cells with 5% Power Conversion Efficiency Using Photonic Crystal Reflector. *ACS Appl. Mater. Interfaces* **2014**, *6*, 599−605.
(6) Tong, M. H.; Coates, N. E.; Moses, D.; Heeger, A. J.; Beaupre, S.; Leclerc, M. Charge Carrier Photogeneration and Decay Dynamics in the Poly(2,7-carbazole) Copolymer PCDTBT and in Bulk Heterojunction Composites with $PC_{70}BM$. *Phys. Rev. B* **2010**, *81*, 12510.
(7) Wakim, S.; Beaupre, S.; Blouin, N.; Aich, B. R.; Rodman, S.; Gaudiana, R.; Tao, Y.; Leclerc, M. Highly Efficient Organic Solar Cells

Based on a Poly(2,7-carbazole) Derivative. *J. Mater. Chem.* **2009**, *19*, 5351−5358.
(8) Wenjuan, Yu; X, J.; Long, Y.; Shen, L.; Yan, L.; Wenbin, G.; Shengping, R. Highly Efficient Semitransparent Polymer Solar Cells with Color Rendering Index Approaching 100 Using One-Dimensional Photonic Crystal. *ACS Appl. Mater. Interfaces* **2015**, DOI: 10.1021/acsami.5b02039.
(9) Lu, L. Y.; Yu, L. P. Understanding Low Bandgap Polymer PTB7 and Optimizing Polymer Solar Cells Based on It. *Adv. Mater.* **2014**, *26*, 4413−4430.
(10) Liang, Y. Y.; Xu, Z.; Xia, J. B.; Tsai, S. T.; Wu, Y.; Li, G.; Ray, C.; Yu, L. P. For the Bright Future-Bulk Heterojunction Polymer Solar Cells with Power Conversion Efficiency of 7.4%. *Adv. Mater.* **2010**, *22*, E135−E138.
(11) Dai, A.; Zhou, Y. H.; Shu, A. L.; Mohapatra, S. K.; Wang, H.; Fuentes-Hernandez, C.; Zhang, Y. D.; Barlow, S.; Loo, Y. L.; Marder, S. R.; Kippelen, B.; Kahn, A. Enhanced Charge-Carrier Injection and Collection Via Lamination of Doped Polymer Layers p-Doped with a Solution-Processible Molybdenum Complex. *Adv. Funct. Mater.* **2014**, *24*, 2197−2204.
(12) An, Q. S.; Zhang, F. J.; Li, L. L.; Wang, J.; Sun, Q. Q.; Zhang, J.; Tang, W. H.; Deng, Z. B. Simultaneous Improvement in Short Circuit Current, Open Circuit Voltage, and Fill Factor of Polymer Solar Cells through Ternary Strategy. *ACS Appl. Mater. Interfaces* **2015**, *7*, 3691−3698.
(13) Khlyabich, P. P.; Burkhart, B.; Thompson, B. C. Compositional Dependence of the Open-Circuit Voltage in Ternary Blend Bulk Heterojunction Solar Cells Based on Two Donor Polymers. *J. Am. Chem. Soc.* **2012**, *134*, 9074−9077.
(14) Ameri, T.; Min, J.; Li, N.; Machui, F.; Baran, D.; Forster, M.; Schottler, K. J.; Dolfen, D.; Scherf, U.; Brabec, C. J. Performance Enhancement of the P3HT/PCBM Solar Cells through NIR Sensitization Using a Small-Bandgap Polymer. *Adv. Energy Mater.* **2012**, *2*, 1198−1202.
(15) Li, X. M.; Xie, D.; Park, H. S.; Zhu, M. T. H. Z.; Wang, K. L.; Wei, J. Q.; Wu, D. H.; Zhu, J. K. Ion Doping of Graphene for High-Efficiency Heterojunction Solar Cells. *Nanoscale* **2013**, *5*, 1945−1948.
(16) Kim, S. M.; Jo, Y. W.; Kim, K. K.; Duong, D. L.; Shin, H. J.; Han, J. H.; Choi, J. Y.; Kong, J.; Lee, Y. H. Transparent Organic P-Dopant in Carbon Nanotubes: Bis(trifluoromethanesulfonyl)imide. *ACS Nano* **2010**, *4*, 6998−7004.
(17) Zhou, Y. H.; Fuentes-Hernandez, C.; Shim, J.; Meyer, J.; Giordano, A. J.; Li, H.; Winget, P.; Papadopoulos, T.; Cheun, H.; Kim, J.; Fenoll, M.; Dindar, A.; Haske, W.; Najafabadi, E.; Khan, T. M.; Sojoudi, H.; Barlow, S.; Graham, S.; Bredas, J. L.; Marder, S. R.; Kahn, A.; Kippelen, B. A Universal Method to Produce Low-Work Function Electrodes for Organic Electronics. *Science* **2012**, *336*, 327−332.
(18) Zhou, H. Q.; Y, Z.; Mai, C. K.; Collins, S. D.; Nguyen, T. Q.; Bazan, G. C.; Heeger, A. J. Conductive Conjugated Polyelectrolyte as Hole-Transporting Layer for Organic Bulk Heterojunction Solar Cells. *Adv. Mater.* **2014**, *26*, 780−785.
(19) Han, X.; Wu, Z.; Sun, B. Enhanced Performance of Inverted Organic Solar Cell by a Solution-Based Fluorinated Acceptor Doped P3HT:PCBM Layer. *Org. Electron.* **2013**, *14*, 1116−1121.
(20) Tunc, A. V.; De Sio, A.; Riedel, D.; Deschler, F.; Da Como, E.; Parisi, J.; von Hauff, E. Molecular Doping of Low-Bandgap-Polymer:Fullerene Solar Cells: Effects on Transport and Solar Cells. *Org. Electron.* **2012**, *13*, 290−296.
(21) Lei, X.; Zhang, F.; Song, T.; Sun, B. P-type Doping Effect on the Performance of Organic-Inorganic Hybrid Solar Cells. *Appl. Phys. Lett.* **2011**, *99*, 233305−3.
(22) Zhang, Y.; Zhou, H. Q.; Seifter, J.; Ying, L.; Mikhailovsky, A.; Heeger, A. J.; Bazan, G. C.; Nguyen, T. Q. Molecular Doping Enhances Photoconductivity in Polymer Bulk Heterojunction Solar Cells. *Adv. Mater.* **2013**, *25* (48), 7038−7044.
(23) Miao, X. C.; Tongay, S.; Petterson, M. K.; Berke, K.; Rinzler, A. G.; Appleton, B. R.; Hebard, A. F. High Efficiency Graphene Solar Cells by Chemical Doping. *Nano Lett.* **2012**, *12*, 2745−2750.
(24) Kim, D.; Lee, D.; Lee, Y.; Jeon, D. Y. Work-Function Engineering of Graphene Anode by Bis(trifluoromethanesulfonyl)-amide Doping for Efficient Polymer Light-Emitting Diodes. *Adv. Funct. Mater.* **2013**, *23*, 5049−5055.
(25) Arkhipov, V. I.; Emelianova, E. V.; Heremans, P.; Bassler, H. Analytic Model of Carrier Mobility in Doped Disordered Organic Semiconductors. *Phys. Rev. B* **2005**, *72*, 235202.
(26) Pingel, P.; Schwarzl, R.; Neher, D. Effect of Molecular P-doping on Hole Density and Mobility in Poly(3-hexylthiophene). *Appl. Phys. Lett.* **2012**, *100*, 143303.
(27) Xiao, Y. B.; Zhou, S.; Su, Y. R.; Ye, L.; Tsang, S. W.; Xie, F. Y.; Xu, J. B. TFSA Doped Interlayer for Efficient Organic Solar Cells. *Org. Electron.* **2014**, *15*, 3702−3709.
(28) Tsang, S. W.; Tse, S. C.; Tong, K. L.; So, S. K. PEDOT: PSS Polymeric Conducting Anode for Admittance Spectroscopy. *Org. Electron.* **2006**, *7*, 474−479.
(29) Tsang, S. W.; So, S. K.; Xu, J. B. Application of Admittance Spectroscopy to Evaluate Carrier Mobility in Organic Charge Transport Materials. *J. Appl. Phys.* **2006**, *99*, 013706.
(30) Lee, H. K. H.; Li, Z.; Constantinou, I.; So, F.; Tsang, S. W.; So, S. K. Batch-to-Batch Variation of Polymeric Photovoltaic Materials: its Origin and Impacts on Charge Carrier Transport and Device Performances. *Adv. Energy. Mater.* **2014**, *4*, 1400768−8.
(31) Chen, S.; Tsang, S. W.; Lai, T. H.; Reynolds, J. R.; So, F. Dielectric Effect on the Photovoltage Loss in Organic Photovoltaic Cells. *Adv. Mater.* **2014**, *26*, 6125−6131.
(32) Tsang, S. W.; Chen, S.; So, F. Energy Level Alignment and Sub-Bandgap Charge Generation in Polymer:Fullerene Bulk Heterojunction Solar Cells. *Adv. Mater.* **2013**, *25*, 2434−2439.

DOI: 10.1021/acsami.5b02104
ACS Appl. Mater. Interfaces 2015, 7, 13415−13421